INVESTIGATION ON STRUCTURAL AND AERODYNAMIC CHARACTERISTICS OF RESONANT TYPE ELASTIC FLAPPING WING

Hiroto Nagai*, Koji Isogai*, Masahiko Murozono, Tsutomu Fujishiro****
***Nippon Bunri University, **Kyushu University**
nagai@nbu.ac.jp; isogai@nbu.ac.jp; murozono@aero.kyushu-u.ac.jp

Keywords: *Micro Air Vehicle, Flapping wing, Aeroelasticity, Numerical Analysis, Design*

Abstract

Structural and aerodynamic characteristics for the two resonant type elastic flapping wings are experimentally and numerically investigated. The numerical simulation of aeroelastic response for the two wings is conducted by the 3D Navier-stokes code considering the modal analysis calculated by FEM. The thrust performance and the vibrational mode are in good agreement between the experimental and numerical results. The aerodynamic responses obtained by the numerical simulation indicate that the two wing models show the preferable wing kinematics with respect to the feathering amplitude and the phase difference between the flapping and feathering motions. On the basis of the numerical estimation, we have selected the appropriate driving motor for the resonant type flapping wing and designed and developed a new prototype of the flapping Micro Air Vehicle, which has four resonant type flapping wings with four driving motors. In the tethered flight test, the prototype succeeded in lifting the body with the weight of 80.8 g except a buttery and motor controller.

1 Introduction

Micro air vehicles (MAVs), which are handheld unmanned aircraft, are expected to be used for rescue, surveillance, exploration, and reconnaissance missions. Insect flight mechanisms have fascinated many researchers as a good candidate for a MAV. Despite of their small sizes, insects have good flight maneuverability and stability even in open air. Their advantage is mainly gained from their flapping wings. The flapping wing kinematics of insects consists of flapping and feathering motions. The flapping motion is a rotational oscillation around a body axis (up- and downstroke), and the feathering motion is a rotational oscillation around a span axis of the wing (supination and pronation). Insects control their wing kinematics appropriately to generate larger lift and thrust. When a MAV mechanically realizes the appropriate flapping kinematics like insects, it needs a complex mechanical link system to drive the wing actively at the wing base, which requires a larger driving torque and causes excessive body weight. Recently, many flapping MAVs have been developed, some of which have attained success of free flight [1, 2]. The light weight technology by micro mechanical engineering has contributed to the success of the flapping type MAVs. However, more powerful flapping MAVs which can carry more payloads are required for future practical missions by autonomous flight.

To solve the problem, we have proposed an idea of resonance type elastic flapping wing, which produces both flapping and feathering motions passively using a resonance phenomenon [3, 4]. When a small flapping oscillation is applied to the wing base near the natural frequency of the elastic wing, both bending and twisting oscillations of the wing occur with higher amplitude due to the resonance phenomenon. If the distributions of rigidity and density of the elastic wing are appropriate, the preferable flapping kinematics, which means the feathering oscillation has

about 90 deg phase difference ahead of the flapping oscillation [5], are attained from the vibration response due to an aeroelastic phenomenon (see Fig. 1). The advantage of the resonance type elastic flapping wing is a simple actuating mechanism to drive a flapping wing.

We have developed resonance type elastic flapping wings as a result of trial and error. The developed flapping wing is composed of a single CFRP (Carbon Fiber Reinforced Plastic) rod and a thin EPP (Expanded Polypropylene) foam plate. The best wing we developed generated a maximum thrust about 35 gf at an applied frequency of 60 Hz with a semi-span length of 110 mm. On the basis of the result, we have developed a prototype of flapping type MAV with the four developed flapping wings (see Fig. 2). The prototype 1 had a weight of 48 g including a body frame, three driving motors, and four flapping wings except a buttery and controller. The prototype 1 did not generate enough thrust beyond the body weight. The mounted small-size motor could not drive the wing at the required flapping frequency; the maximum flapping frequency driven by the mounted motor was 33 Hz. An appropriate driving motor for a flapping type MAV should have high torque performance to drive the wing at a higher flapping frequency in addition to a small-size and light weight. To select a motor appropriately, we need to estimate the thrust and torque performance of the elastic flapping wing with respect to the flapping frequency.

The aerodynamic performance of the resonant type elastic flapping wing is dominated by many parameters: planform, distributions of rigidity and density, applied vibration, and so on. These parameters influence the aeroelastic response of the flapping wing. Recently, the characteristics of flexible flapping wings, such as membrane, have been investigated by many researchers [6-9]. However, the structural and aerodynamic characteristics for the elastic flapping wing using a resonant phenomenon have not been investigated. Since we have developed the resonant type elastic flapping wing by trial and error, the design of the wing is not still optimized. For investigation of the wing characteristics and optimization of the structural design of the wing, numerical simulation for the resonant type elastic flapping wing are required.

In this study, Numerical aeroelastic simulation is conducted for resonant type elastic flapping wing. We experimentally and numerically investigate structural and aerodynamic characteristics for two models of the resonance type elastic flapping wing, which show better performance in the wings we have developed. In the experimental study, vibrational mode and time-averaged thrust generated by flapping oscillation are measured for the two wing models. In the numerical simulation, we conduct vibration modal analysis using FEM (finite element method) and aeroelastic analysis using CFD (computational fluid dynamics) based on 3D Navier-Stokes code considering the structural characteristics of the wing.

In Section 3, we compare the experimental and numerical results for validation of our methods. In Section 4, we investigate and discuss the vibrational mode, thrust performance with respect to the flapping frequency, and aeroelastic responses during a flapping oscillation for the two wings. In Section 5, we select an appropriate motor for driving the resonant type elastic flapping wing, based on the numerical estimation. Moreover, we design and develop a new prototype of the flapping MAV based on the numerical estimation. A tethered flight test of the developed prototype is conducted for validation of the numerical estimation.

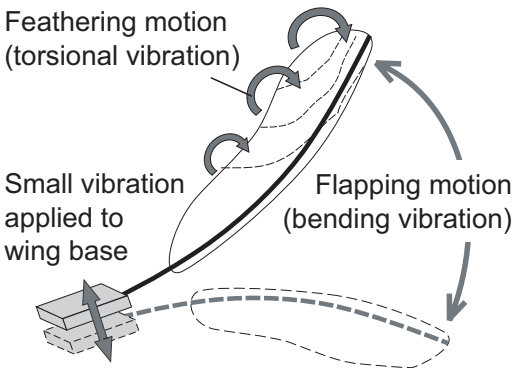

Fig. 1. Resonant type elastic flapping wing

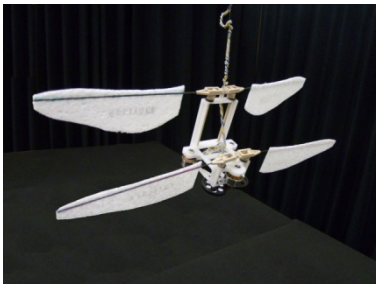

Fig. 2. Prototype 1 with four resonant type flapping wings

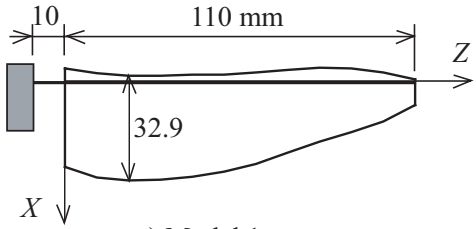

a) Model 1

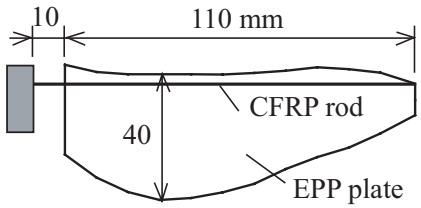

b) Model 2

Fig. 3. Planforms of two wing models

2 Materials and Methods

2.1 Experimental Method

Two models of the resonant type flapping wing are used in this study. The resonant type elastic flapping wing consists of a single CFRP rod and a thin EPP foam plate with the expansion ratio of 30 times. The CFRP rod is fixed on the EPP plate using adhesive. The planform of the model 1 is derived from a hindwing of a dragonfly, *Onychogomphus viridicostus*, as illustrated in Fig. 3a. The model 2 is expanded 1.2 times to chord direction from the model 1 and cut off slightly around the trailing edge of the wing base, as illustrated in Fig. 3b. The CFRP rod has a diameter of 1.0 mm for the model 1 and 1.2 mm for the model 2. The EPP plate has a thickness of 1.5 mm for the model 1 and 2.0 mm for the model 2. The CFRP rod was fixed as a cantilever beam at 10 mm apart from the EPP plate.

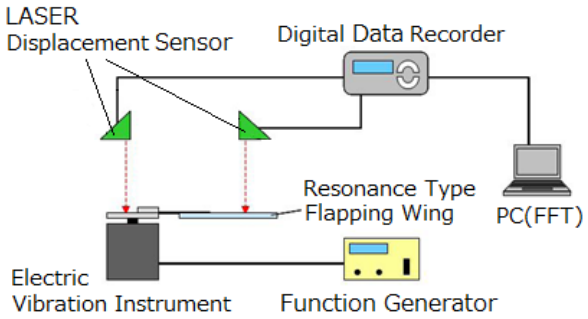

Fig. 4. Measurement system of vibrational mode

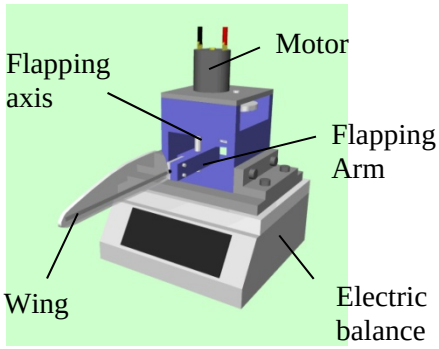

Fig. 5. Vibration test bet for measurement of thrust of flapping wing

To obtain the natural frequencies and vibrational mode shapes of the wings, vibration response of the two wings were measured using laser displacement meters when small sinusoidal oscillation was applied to the wing base, as shown in Fig. 4. The wing rod was fixed on the electric vibration instruments, which applied a small sinusoidal displacement oscillation to the wing base. There were 25 points of measurement on the wing plate (5 points along the chord direction at 5 sections along the wing span). The displacement at the two points (a measurement point on the wing and the wing base) were measured at the same time using two laser displacement meters. The two voltage signals from the laser displacement meters were input to a digital data recorder and calculated by a FFT analyzer to obtain frequency response functions. First, the frequency responses at two measurement points (at trailing-edges of 50% and 75% semi-span locations) were measured by sweeping the frequency with 1 Hz increments from 10 to 300 Hz. From the measured frequency responses, we determined

the four natural frequencies from the first to the fourth. Secondly, frequency response functions at 25 points on the wing plate were measured at each natural frequency. From the measured frequency response functions, we obtained a mode shape of the wing at each natural frequency.

Thrust measurement was made using the test bet shown in Fig. 5. The wing rod was fixed at a flapping arm of the test bet apart from 10 mm from the wing plate. The flapping arm with a length of 30 mm from the flapping axis was oscillated horizontally by a motor at amplitude of 10 deg. When the leading-edge of the wing is vertically downward, the thrust generated by the flapping wing is directed vertically downward. The test bed was placed on an electric balance to measure the time-averaged thrust generated by the flapping wing. At the same time, the flapping frequency was measured using a laser displacement meter pointing to the flapping arm. The thrust measurement was made for the four wings of each wing model, and the averaged data was obtained.

2.2 Numerical Method

Numerical vibration modal analysis was conducted using ANSYS 14.0 for FEM analysis. Beam elements and plate elements were used to model the CFRP rod and EPP plate, respectively. The material properties are as follows; Young's modulus is 108.5 GPa for CFRP and 1.11 MPa for EPP; the density is 1500 kg/m^3 for CFRP and 31.66 kg/m^3 for EPP; Poisson's ratio is 0.3.

On the basis of the vibrational modal analysis, we conducted numerical aeroelastic simulation using a 3D Navier-stokes code developed by Isogai et al. [3, 4], which considers the vibrational mode shapes with FEM analysis. The displacement F of the wing normal to the wing surface is expressed as

$$F(X,Z,t) = F_R(X,Z,t) + \sum_{i=1}^{N} H_i(X,Z) q_i(t) \tag{1}$$

where t is time, Z is the spanwise coordinate, X is the chordwise coordinate, as shown in Fig. 2a, q_i is the generalized coordinate, and H_i is the natural vibrational mode shapes of the wing. The four mode shapes obtained by the FEM analysis is substituted to H_i; therefore, N = 4. F_R in Eq. (1) is the displacement of the forced oscillation as defined by

$$F_R(X,Z,t) = (R_r + \phi_0 Z)\sin(\omega t) \tag{2}$$

where R_r is the displacement of the wing at root section and ϕ_0 is the flapping amplitude. Using Lagrange's equations of motion, we obtain the ordinary differential equations of motion for q_i as follows:

$$\begin{aligned} &M_i\ddot{q}_i + (\omega_i^2/\omega) g_i M_i \dot{q}_i + \omega_i^2 M_i q_i \\ &= -\iint_S m(X,Z) H_i(X,Z) \frac{d^2 F_R(X,Z,t)}{dt^2} dXdZ \\ &\quad + \iint_S \Delta P(X,Z,t) H_i(X,Z) dXdZ \\ &\qquad\qquad (i = 1, N) \end{aligned} \tag{3}$$

where M_i is the generalized mass; ω_i is the natural frequency; ω is the frequency of excitation; g_i is the damping coefficient; m is the mass per unit area of the wing surface; and ΔP is the pressure difference computed using the 3D Navier-Stokes code. Equations coupled with the 3D Navier-Stokes equation are solved at each time step to obtain the aeroelastic responses of the wing.

3 Comparison between Experimental and Numerical Results

3.1 Comparison of Vibrational Mode

The experimental and numerical results of natural vibration frequencies and mode shapes for the model 1 are shown in Figs. 6a and 6b, respectively. For the experimental results, the 1st mode shape is spanwise bending at 48 Hz, the 2nd is chordwise bending at 84 Hz, the 3rd is spanwise torsion at 139 Hz, and the 4th corresponds with the 2nd mode of plate vibration at 186 Hz. On the other hand, for the numerical results, the 1st mode shape is chordwise bending at 54.3 Hz, the 2nd is spanwise bending coupled with chordwise bending at 64.4 Hz, the 3rd corresponds with the 2nd mode of plate vibration at 99.1 Hz, and the 4th corresponds with the 3rd mode of plate vibration at 154 Hz. The 2nd mode of the

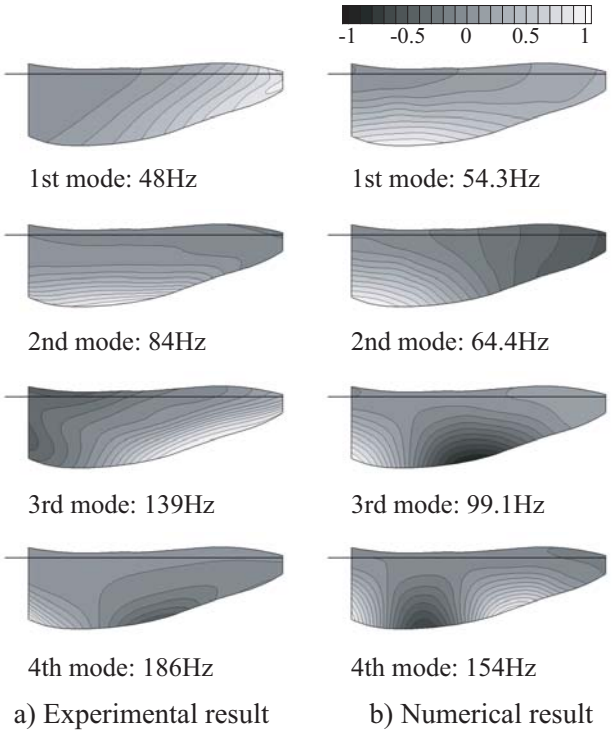

Fig. 6. Vibrational mode shapes for model 1

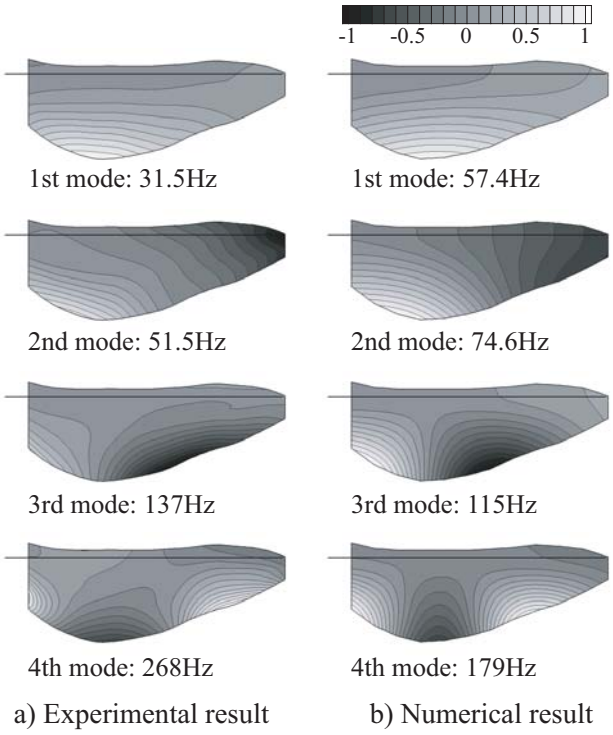

Fig. 7. Vibrational mode shapes for model 2

experimental result is similar to the 1st of the numerical one; and the 4th mode of the experimental result is similar to the 3rd of the numerical one. The 1st and 3rd modes of the experimental result do not appear for the numerical mode shapes. The natural frequencies for the experimental and numerical results do not agree well except for the 1st natural frequencies.

The experimental and numerical results of natural frequencies and mode shapes for the model 2 are shown in Figs. 7a and 7b, respectively. For the experimental results, the 1st mode shape is the chordwise bending at 31.5 Hz, the 2nd is spanwise bending coupled with chordwise bending at 84 Hz, the 3rd corresponds with the 2nd mode of plate vibration at 137 Hz, and the 4th corresponds with the 3rd mode of plate vibration at 268 Hz. The each mode shape of the numerical result agrees well with that of the experimental result, although the natural frequencies do not agree well each other.

The mode shapes for the model 2 agree well between the experimental and numerical results, while those for the model 1 disagree. It is likely that the disagreement for the model 1 is attributed to the influence of air because the model 1 is a smaller size and lighter weight than the model 2.

3.2 Comparison of Thrust performance

The time-averaged thrust with respect to the flapping frequency for the model 1 is shown in Fig. 8. Thrust has a maximum of 18.7 gf at 45.9 Hz for the experimental result and 14.8 gf at 50 Hz for the numerical result, at which the model 1 has the 1st natural frequency. Although thrust value for the numerical result is higher than that for the experimental result, the tendency of thrust performance is similar between the experimental and numerical results. In the experiment, the CFRP rod was broken from the fixed end at near 50 Hz.

The thrust performance for the model 2 is shown in Fig. 9. Thrust has a maximum of 35.9 gf at 57.9 Hz for the experimental result, 33.9 gf at 60 Hz for the numerical result. As is the case with the model 1, the maximum thrust for the model 2 is generated around the 1st natural frequency for the numerical result. Since the mode shapes for the numerical results are in good agreement with those for the experimental

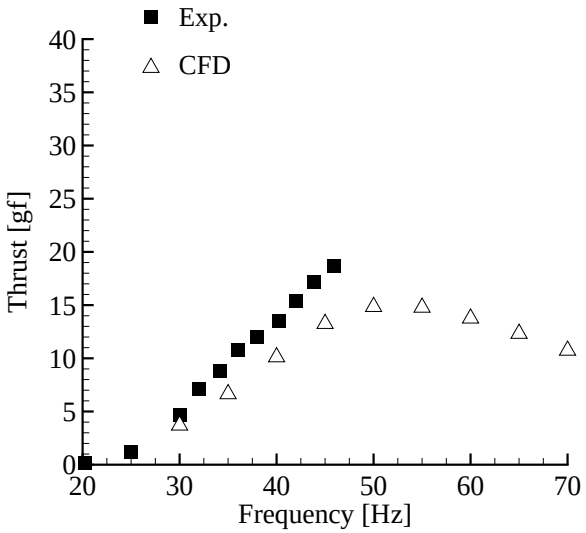

Fig. 8. Thrust performance with respect to the flapping frequency for model 1

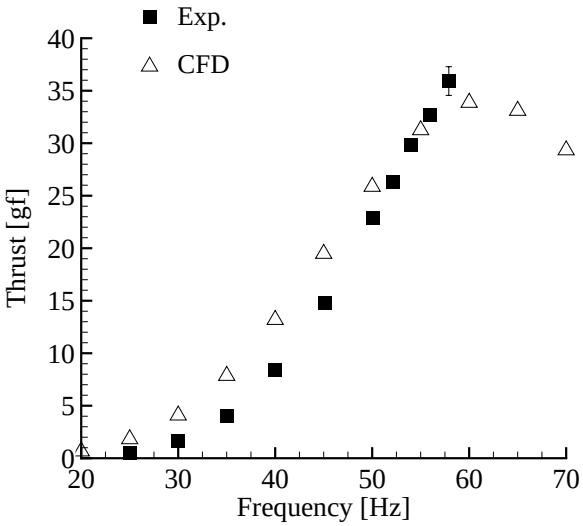

Fig. 9. Thrust performance with respect to the flapping frequency for model 2

results, the numerical estimation of thrust performance for the model 2 also agrees well with the experimental result.

4 Investigation of Aeroelastic Response

We investigate the aeroelastic responses of the resonant type elastic flapping wing calculated by the numerical simulation when the maximum thrust is generated. The time histories of thrust, flapping and feathering responses, and generalized coordinates for one flapping cycle are shown in Fig. 10 for the model 1 at 50 Hz and in Fig. 11 for the model 2 at 60 Hz. Note that Figs. 10b and 11b show the time history of flapping and feathering angles at the 50% semi-span location, and the generalized coordinate is non-dimensionalized by the reference length, that is the semi-chord length at 75% semi-span location.

As shown in Fig. 10b, the amplitude of the flapping vibration at 50% semi-span is 19.8 deg, the amplitude of the feathering vibration is 49.9 deg, and the phase difference of feathering vibration is 112 deg ahead of the flapping vibration. As shown in Fig. 11b, the amplitude of the flapping vibration is 20.9 deg, the amplitude of the feathering vibration is 58.2 deg, and the phase difference of the feathering vibration is 95.1 deg ahead of the flapping vibration. Although the amplitude of the flapping vibration is the same in the two wing models, the amplitude of the feathering vibration and the phase difference are different in the two models. From the previous research for rigid, flat-plate flapping wings [5], it is preferable for a rigid flapping wing that the amplitude of feathering angle is from 45 to 60 deg, and the phase difference is from 90 to 110 deg, from a standpoint of high thrust and efficiency. Therefore, the aeroelastic responses at 50% semi-span for the two models are preferable for the purpose of larger thrust generation.

In the case with a rigid flapping wing, thrust absolutely becomes zero at a certain moment, generally around the stroke reversal, because the feathering angle becomes zero at that time [5]. On the other hand, as can be seen in Figs. 10a and 11a, the two models generates positive thrust all through the flapping cycle. This fact is one of the notable features of the resonant type elastic flapping wings. To investigate the reason, the aerodynamic response for the model 2 and the vortex pattern around the wing are shown in Fig. 12, where the wing moves from the right to left stroke. In this figure, the red and blue contours show the vorticity with counter-clockwise and clockwise rotations, respectively. Let us focus on the non-

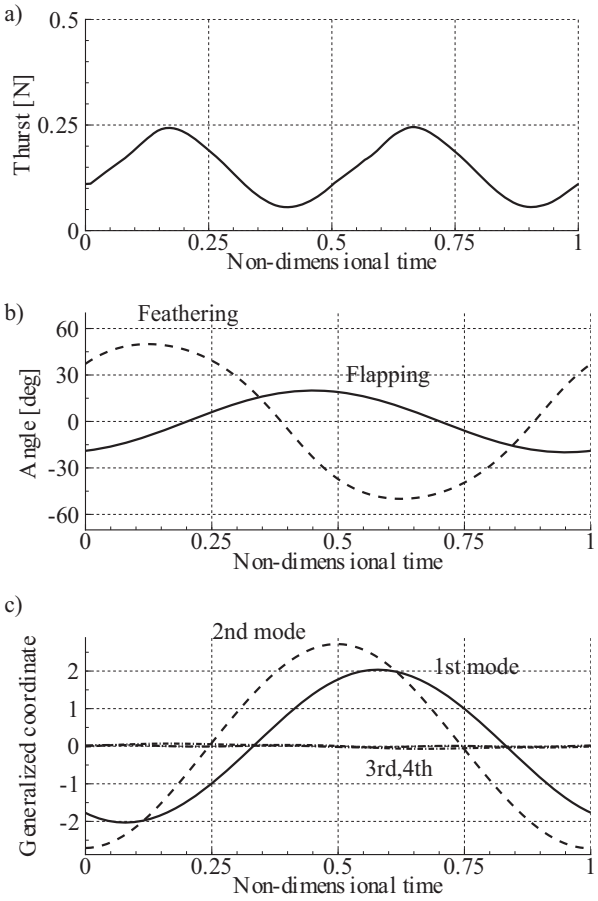

Fig. 10. Time histories of thrust, flapping and feathering angles, and generalized coordinate for model 1 at the flapping frequency of 50 Hz

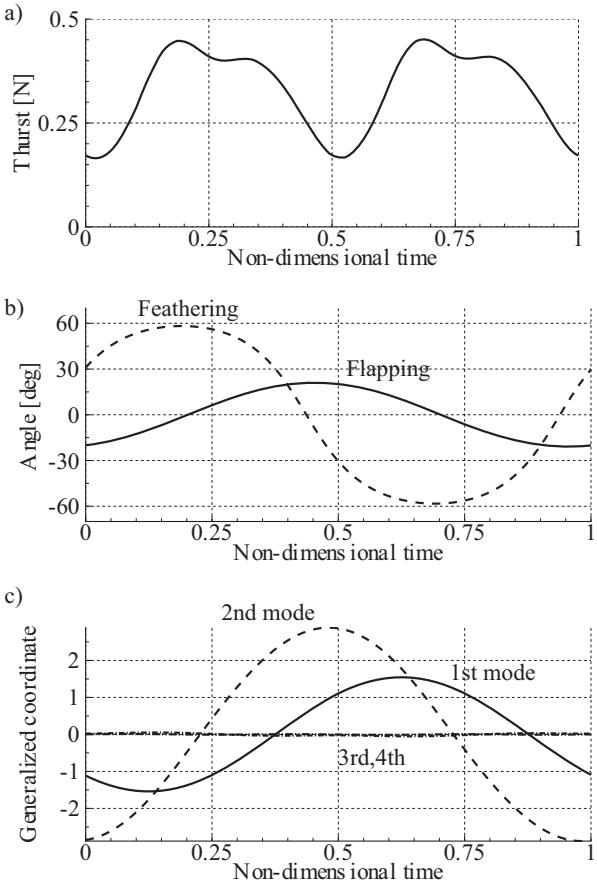

Fig. 11. Time histories of thrust, flapping and feathering angles, and generalized coordinate for model 2 at the flapping frequency of 60 Hz

dimensional time t^* = 0.5, when the wing generates the minimum thrust around the stroke reversal. In the right stoke, the leading-edge vortex (red) is attached on the wing upper surface. At the stroke reversal (t^* = 0.5), the opposite torsional responses occur between the wing tip and base. At the wing base, the feathering angle is still positive, and the leading-edge vortex (red) produced during the right stroke still remains. At the wing tip, the feathering angle is negative, and the new leading-edge vortex (blue) is produced. The wing instantaneous deformation which has the opposite phase between the wing tip and base corresponds with the 2nd mode shape shown in Fig. 7. Due to the 2nd mode shape, the wing always has an appropriate angle of attack somewhere along the wingspan. Therefore, the wing generates positive thrust all through the flapping cycle.

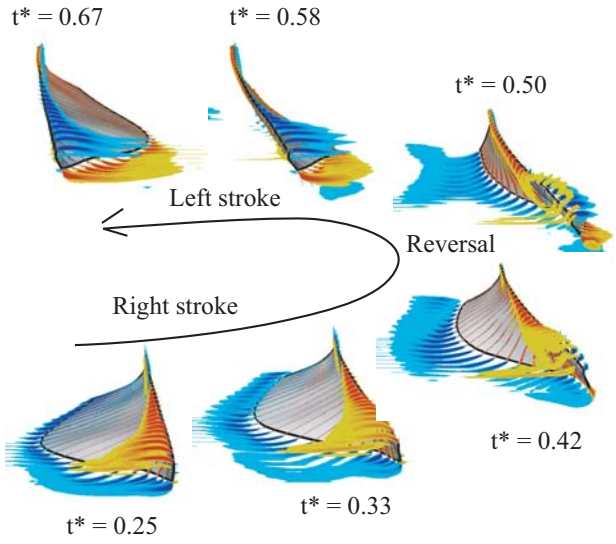

Fig. 12. Aeroelastic responses and vortices around flapping wing for model 2 by numerical simulation

5 Development of Resonant type Flapping MAV

On the basis of the numerical estimation for the resonant type elastic flapping wing, we have designed and developed a new prototype of flapping type MAV. The wing model 2 was employed for the new prototype because the numerical estimation for the model 2 is in good agreement with the experimental results. Two types of out-runner brushless DC motors, which produce high torque with a small-size, were a candidate to drive the resonant type elastic flapping wing: motor 1 (CT1411-2000) and motor 2 (CT1811-2900, Cosmo-Tech Co., Japan). The motor torque/speed curves for the motor 1 and motor 2 with applied voltage of 7.5 V are shown in Figs. 13 and 14, respectively, in addition to the wing torque curve for the model 2 calculated by numerical simulation. Note that the motor torque curves include the effect of a gear and a crank, which converts the motor rotation to reciprocating flapping motion. Therefore, the motor torque curves varies with the amplitude of the flapping angle applied to the wing base: 10, 12, 14, 16, and 18 deg. The intersections of the wing and motor curves mean the estimation of the maximum driving flapping frequency. There is optimal flapping amplitude applied to the wing base to maximize thrust generation. Although the optimal amplitude of applied flapping angle is 14 deg for both motors, we employ the amplitude of 12 deg. When the motor 1 is used at the amplitude of 12 deg, the maximum flapping frequency is 33 Hz, and the maximum thrust is 9 gf. For the motor 2, the maximum flapping frequency is 44 Hz, and the maximum thrust is 25 gf. The prototype 1 (Fig. 2) had four wings of the model 2 at the flapping amplitude of 12 deg driven by the motor 1. Since the total thrust is 36 gf from the numerical estimation, the prototype 1 with the body weight of 48g cannot obviously fly. When the motor 2 is employed with the flapping amplitude of 12 deg, the total thrust of 100 gf is expected.

We have designed and developed prototype 2 with four wings of the wing model 2 driven by the motor 2 with the applied flapping amplitude of 12 deg. The 3D design of the prototype 2 is shown in Fig. 15. The prototype 2

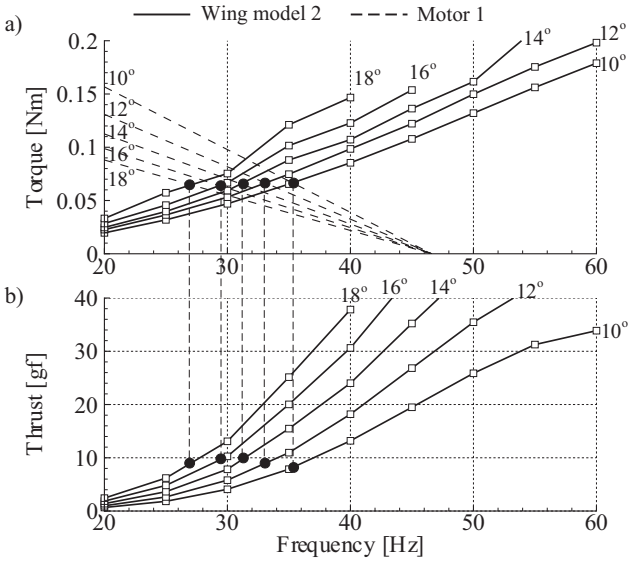

Fig. 13. Torque curves for the motor 1, and torque and thrust curve for wing model 2

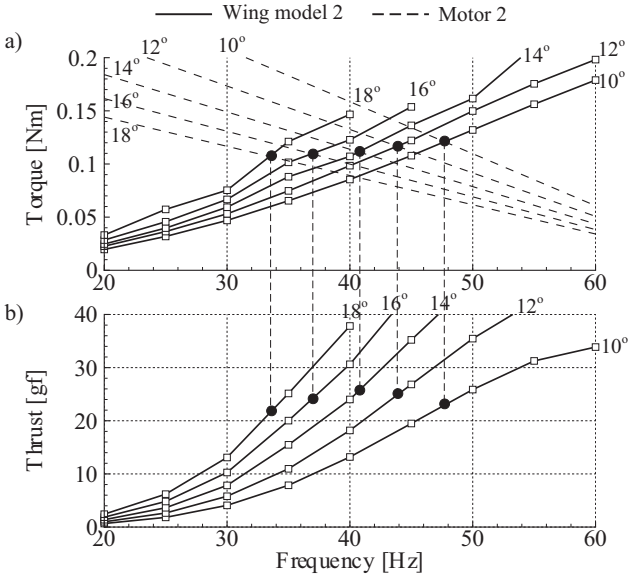

Fig. 14. Torque curves for the motor 2, and torque and thrust curve for wing model 2

had four motors, which independently control the flapping frequency of each flapping wing. The four flapping wings were arranged in X-shape in order to increase the pitching and rolling moment around the body produced by the four flapping wings in terms of the maneuverability. The rotating speeds of the motors are controlled manually by radio control system. The four electronic speed controllers for each brushless motor, a buttery, and a receiver

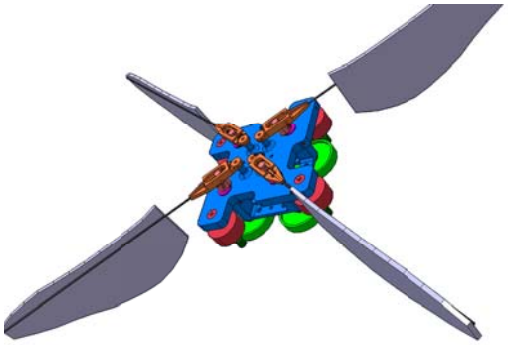

were not mounted but placed on the ground. The developed prototype 2 is shown in Fig. 16. The body weight is 80.8 g, including the body frame, four flapping wings, four motors, gears, and cranks; the size is 22.8 cm × 22.3 cm. The flapping frequency for the wing model 2 driven by the motor 2 was measured using a strobe light. The maximum flapping frequency was 43 Hz, which agrees well with the numerical estimation shown in Fig. 14a. The tethered flight test for the prototype 2 was conducted. Although the flight control was difficult, the prototype 2 lifted the body by the four resonant type elastic flapping wings.

6 Conclusions

We have measured the structural and aerodynamic characteristics for the two resonant type elastic flapping wings. The numerical simulation of aeroelastic response for the two wings has been conducted by the 3D Navier-stokes code considering the modal analysis calculated by FEM. The thrust performance and the vibrational mode were in good agreement between the experimental and numerical results. The aerodynamic responses obtained by the numerical simulation indicate that the two wing models show the preferable wing kinematics with respect to the feathering amplitude and the phase difference between the flapping and feathering motions. On the basis of the numerical estimation, we have selected the appropriate driving motor for the resonant type flapping wing and designed and developed the new prototype of the flapping MAV, which has four resonant type flapping wings with four driving motors. In the tethered flight test, the prototype succeeded in lifting the body with the weight of 80.8 g except the buttery and motor controller. In the future work, we will optimize the wing structure of the resonant type flapping wing for high performance using the numerical aeroelastic simulation. For the wireless flight with a buttery and controller, we will improve the design of the prototype.

Acknowledgement

This study was supported by Japan Society for the Promotion of Science (JSPS) KAKENHI Grant-in-Aid for Young Scientists (B).

References

[1] Lentink D, Jongerius SR, and Bradshaw NL. The Scalable Design of Flapping Micro-Air Vehicles Inspired by Insect Flight. *Control*, Spriger-Verlag, Berlin, 2009, Chapter 14, pp 185-205.

[2] Keennon M, Klingebiel K, Won H, and Andriukov A. Development of the Nano Hummingbird: A Tailless Flapping Wing Micro Air Vehicle. *Proc 50th AIAA*

Aerospance Science Meeting including the New Horizons Forum and Aerospace Exposition, Nashville, Tennessee, AIAA 2012-0588, 2012.

[3] Isogai K, Kamisawa Y and Sato S. Resonance Type Flapping Wing for Micro Air Vehicle. *Trans. of the Japan Soc. for Aeronautical and Space Science*, Vol. 52, No. 178, pp 199-205, 2010.

[4] Isogai K and Kawabe H. Transition Flight Simulation of Flapping-Wing Micro-Aerial Vehicle Using Aerodynamic Database. *Trans. of the Japan Soc. for Aeronautical and Space Science*, Vol. 53, No. 180, pp 138-146, 2010.

[5] Nagai H and Isogai K. Effects of Flapping Wing Kinematics on Hovering and Forward Flight Aerodynamics. *AIAA Journal*, Vol. 49, No. 8, pp 1750-1762, 2011.

[6] Gopalakrishnan P and Tafti DK. Effect of Wing Flexibility on Lift and Thrust Production in Flapping Flight. *AIAA Journal*, Vol. 8, No. 5, pp 865-877, 2010.

[7] Bansmer S, Radespiel R, Unger R, Haupt M, Horst P. Experimental and Numerical Fluid-Structure Analysis of Rigid and Flexible Flapping Airfoils. *AIAA Journal*, Vol. 48, No. 9, pp 1959-1974, 2010.

[8] Wu P, Ifju P, and Stanford B. Flapping Wing Structural Deformation and Thrust Correlation Study with Flexible Membrane Wings. *AIAA Journal*, Vol. 48, No. 9, pp 2111-2122, 2010.

[9] Yang T, Wei M, and Zhao H. Numerical Study of Flexible Flapping Wing Propulsion. *AIAA Journal*, Vol. 48, No. 12, pp 2909-2915, 2010.

Copyright Statement